

A Self-consistent Numerical Study of the Global Solar Wind Driven by the Unified Nonlinear Alfvén Wave

L.P. Yang^{1,2} · X.S. Feng¹ · J.S. He² · L. Zhang¹ ·
M. Zhang¹

Received: 13 August 2015 / Accepted: 30 January 2016 / Published online: 18 February 2016
© Springer Science+Business Media Dordrecht 2016

Abstract The global solar wind has been revealed *via in situ* observations to consist of two populations, *i.e.* the tenuous fast solar wind and the dense slow solar wind. Here, we present a self-consistent modeling of the global solar wind driven by the unified nonlinear Alfvén wave. Considering polytropic closure of magnetohydrodynamics instead of isothermal assumption, the low-frequency Alfvén waves with a broadband spectrum are globally injected at the base of the corona, with the amplitude independent of latitude. In our 2.5 dimensional model, the presence of the Alfvén waves is identified overall in a region away from the equatorial plane, and the waves significantly accelerate the plasma therein to form the fast wind. Near the equatorial plane, a slow wind is generated, and the slowness can be attributed to the absence of Alfvén waves owing to the strong damping at lower altitude. The velocity ratio of both modes, if extrapolated to 1 AU, conforms to the measurements. Far from the Sun, however, the temperature of the fast wind is lower than that of its surroundings, indicating that shock-heating might be inadequate and other mechanisms are probably required to heat the fast wind, such as the dissipation of Alfvénic turbulence.

Keywords Magnetohydrodynamics · Solar wind, theory · Waves, Alfvén

✉ L.P. Yang
lpyang@spaceweather.ac.cn
X.S. Feng
fengx@spaceweather.ac.cn
J.S. He
jshept@gmail.com
L. Zhang
lzhang@spaceweather.ac.cn
M. Zhang
mzhang@spaceweather.ac.cn

¹ SIGMA Weather Group, State Key Laboratory for Space Weather, National Space Science Center, Chinese Academy of Sciences, 100190 Beijing, China

² School of Earth and Space Sciences, Peking University, 100871 Beijing, China

1. Introduction

In the solar wind, two populations of outflow are observationally identified: a fast solar wind flowing at $700\text{--}800\text{ km s}^{-1}$ at 1 AU, and a slow solar wind with a speed of $300\text{--}400\text{ km s}^{-1}$. Commonly, especially at solar activity minima, the fast solar wind mainly comes from polar coronal holes with open magnetic field structures; the slow wind appears to originate from equatorial coronal streamers with closed magnetic field structures. In the white-light images of the corona, the former is dark and the latter bright (McComas *et al.*, 2000). In addition, the fast solar wind is relatively steady, uniform, and the fluctuations embodied are observed to possess the properties of Alfvén waves (Tu and Marsch, 1995; McComas *et al.*, 2003; Wang *et al.*, 2012). As the slow solar wind is associated with the tapering of the streamers into stalks, it is highly variable, intermittent, and Alfvénic fluctuations therein are weaker (Woo and Martin, 1997; Grappin, Léorat, and Buttigheffer, 2000).

To reproduce the fast and slow solar wind, many theoretical and computational models have been proposed – see the reviews by Hollweg (2006), Ofman (2010), and Cranmer (2012). In those models, the acceleration of the slow solar wind was understood in terms of thermal expansion of hot coronal plasma into the interplanetary space, *i.e.* Parker’s thermal expansion model, with an additional source of momentum or energy introduced to explain the fast solar wind. Since outward-propagating Alfvén waves are most prominent in the fast solar wind (Belcher and Davis, 1971), it is thought to be a possible accelerator, and extensive studies have been conducted in numerical simulations (Alazraki and Couturier, 1971; Belcher, 1971; Hollweg, 1973, 1978, 1990; Jacques, 1977; Isenberg and Hollweg, 1982; Davila, 1985; Esser *et al.*, 1986; Barnes, 1992; Ofman and Davila, 1995, 1997, 1998; Lau and Siregar, 1996; Usmanov *et al.*, 2000; Chen and Hu, 2001; Grappin, Léorat, and Habbal, 2002; Li *et al.*, 2004; Ofman, 2004; Suzuki and Inutsuka, 2005; He, Tu, and Marsch, 2008; Cranmer, van Ballegoijen, and Edgar, 2007; Evans *et al.*, 2012; Oran *et al.*, 2013; Matsumoto and Suzuki, 2014).

Noting that the waves exert an Ampere force of second-order magnitude proportional to the gradient of squared wave amplitude (*i.e.* the gradient of wave pressure) on the wind plasma, Belcher (1971) and Alazraki and Couturier (1971) inaugurated the concept of the wave-driven wind. In addition to the bulk acceleration due to Alfvén waves, Hollweg (1973) further investigated the heating though nonlinear wave damping, albeit in an artificial fashion, in a two-fluid solar wind model to explain the high-speed and hot protons observed in the fast wind far from the Sun. Esser *et al.* (1986) discussed the effects of Alfvén waves on the solar wind density profile, flow velocity, and the random motion of protons. They compared the model results to the simultaneous observations of the electron density profile and the resonantly scattered Lyman α line. With the resistive, low- β , two-dimensional (2D) magnetohydrodynamic (MHD) equations in a slab geometry, Ofman and Davila (1995) numerically investigated the heating and acceleration by the fast mode and shear Alfvén waves in coronal holes. Usmanov *et al.* (2000) incorporated the acceleration and heating effects of Alfvén waves into a global solar wind model and successfully reproduced the measurement by the *Ulysses* spacecraft during its first latitude traversal. With the help of Space Weather Modeling Framework (SWMF), Oran *et al.* (2013) incorporated the effects of Alfvén wave heating and acceleration into a global 3D MHD solar wind model with a unified treatment of open and closed magnetic field topologies. However, the models mentioned above were conducted either with linear waves or with the Wentzel–Kramers–Brillouin (WKB) (*i.e.* short-wavelength) approximation, and in global simulations, the wave amplitude is assumed arbitrarily to be related to the magnetic field.

To investigate the acceleration in a complete and self-consistent manner, Ofman and Davila (1997, 1998) developed a nonlinear Alfvén-wave-driven solar wind model in a coronal hole. Their model treated waves as fluctuations in variables in MHD equations, and hence it was capable of evaluating the effects of the wind on the waves, as well as the nonlinear interaction between MHD waves of different types. From the simulation results, they found that solitary waves are driven by the Alfvén wave and contribute significantly to the acceleration of the solar wind in coronal holes. Ofman (2004) extended this explicit contribution of nonlinear Alfvén waves to a three-fluid, thermally conductive and dissipative model of the coronal hole plasma. It should be noted that their models dealt only with the fast solar wind. To include both the fast and slow solar wind in a unified model, Grappin, Léorat, and Habbal (2002) carried out the first global simulations with explicit nonlinear Alfvén wave as a driver. Within the framework of isothermal MHD, they injected a latitude-independent monochromatic Alfvén wave, showing that the injected Alfvén wave leads to a large acceleration of the solar wind. However, the wave has a root-mean-square (rms) amplitude of $\approx 150 \text{ km s}^{-1}$, approaching the observed upper bounds, and the injection is away from the coronal base. Meanwhile, the ratio of the fast and slow wind speeds at $16 R_s$ is still not as large as the observed value, if extrapolated.

In the present study, we revisit the global wave-driven solar wind model with a self-consistent description of waves and a polytropic pressure closure. The low-frequency waves, having a broadband, latitude-independent spectrum, are injected directly at the base of the corona. Great care has been taken to use a fine grid resolution to resolve the waves in a physically plausible manner. Our model reproduces the fast and slow wind well; the ratio of their speeds is conform with *in situ* measurements (if extrapolated to 1 AU). Their temperatures are not as well distinguished in the model, however.

In Section 2 we specify the numerical MHD model. In Section 3 we present the model results, with the fast and slow solar wind clearly distinguished. The differences of two modes are explained therein. In Section 4 we briefly summarize the model and further discuss the heating of the fast solar wind.

2. Numerical MHD Model

The details of the numerical MHD model used here have been described by Feng, Zhang, and Zhou (2014). In this section, only the model features and modifications specific to this study are given. The basic equations are in the non-dimensional form

$$\frac{\partial \rho}{\partial t} + \nabla \cdot \rho \mathbf{u} = 0, \quad (1)$$

$$\frac{\partial \rho \mathbf{u}}{\partial t} + \nabla \cdot \left[\rho \mathbf{u} \mathbf{u} + \mathbf{I} \left(p + \frac{1}{2} \mathbf{B}^2 \right) - \mathbf{B} \mathbf{B} \right] = \rho \mathbf{F}_0, \quad (2)$$

$$\frac{\partial e}{\partial t} + \nabla \cdot \left[\mathbf{u} \left(e + p + \frac{1}{2} \mathbf{B}^2 \right) - (\mathbf{u} \cdot \mathbf{B}) \mathbf{B} \right] = \rho \mathbf{u} \cdot \mathbf{F}_0, \quad (3)$$

$$\frac{\partial \mathbf{B}}{\partial t} + \nabla \cdot (\mathbf{u} \mathbf{B} - \mathbf{B} \mathbf{u}) = 0, \quad (4)$$

where

$$e = \frac{1}{2} \rho \mathbf{u}^2 + \frac{p}{\gamma - 1} + \frac{1}{2} \mathbf{B}^2. \quad (5)$$

Here, ρ is the mass density, \mathbf{u} is the velocity, p is the thermal pressure, and \mathbf{B} is the magnetic field. Time is denoted as t , and \mathbf{r} represents the position vector originating at the center of the Sun. The polytropic index γ is set to be 1.05. In the source term, the external force $\mathbf{F}_0 = -\frac{GM_s}{r^3}\mathbf{r}$ is the solar gravity. G and M_s are the gravity constant and the mass of the Sun, respectively.

To normalize the MHD equations, we used three independent parameters; solar radius R_s , density ρ_s , and acoustic speed a_s at the coronal base. Other variables were normalized by their combinations. The simulation in this article was carried out in 2.5 dimension, and the computational region extends from 1 to 16 R_s in the r -direction, and from the pole to the equator in the θ -direction. The grid spacings are $\delta r = 0.01 R_s$ and $\delta\theta = 0.25$. Parker's hydrodynamic isothermal solar wind solution was employed to give the initial distributions of the plasma density ρ , pressure p , and velocity \mathbf{u} . A dipole field was used for the initial magnetic field to simplify the model. Here, the initial temperature and number density at the coronal base were prescribed to be 1.1×10^6 K and $1 \times 10^8 \text{ cm}^{-3}$ and the initial magnetic field at the pole of the coronal base had a magnitude of 15 gauss (G).

Boundary conditions were set as follows. Along $\theta = 0^\circ$ and $\theta = 90^\circ$, the symmetric boundaries were applied. At the outer boundary of $r = 16 R_s$, a linear extrapolation was implemented since the flow is supersonic and super-Alfvénic. At the inner boundary of $r = 1 R_s$, we fixed all the variables except for the ϕ components of velocity and magnetic field (V_ϕ, B_ϕ), which were set according to the polarization of the Alfvén wave. Like Ofman (2004), a broadband Alfvén wave driver with an ω^{-1} power spectrum was injected as

$$V_\phi(t, \theta, r = 1) = V_d/a_s F(t, \theta), \quad (6)$$

$$B_\phi(t, \theta, r = 1) = -\text{sign}(B_r)V_\phi\sqrt{\rho}, \quad (7)$$

$$F(t, \theta) = \sum_{i=1}^N a_i \sin(\omega_i t + \Gamma_i(\theta)), \quad (8)$$

where $a_i = i^{-0.5}$, $\omega_i = \omega_1 + (i - 1)\Delta\omega$, $\Delta\omega = (\omega_N - \omega_1)/(N - 1)$, $\Gamma_i(\theta)$ is a random phase, $\omega_1 = 0.0006 \text{ rad s}^{-1}$ (corresponding to a period of about 10^4 s), $\omega_N = 100\omega_1$ (corresponding to a period of about 100 s), and the number of modes $N = 400$. The parameter V_d was chosen to be 75 km s^{-1} , complying with the value used by Ofman (2004) and also with the observations.

To solve these equations, a semi-discrete central scheme in spherical coordinates was employed, in which the MHD equations are split into a fluid part and a magnetic part (Ziegler, 2011; Feng, Zhang, and Zhou, 2014). A Godunov-type finite-volume method with magnetic forces as source terms was used for the fluid part and a constrained-transport method to keep $\nabla \cdot \mathbf{B} = 0$ was used for the magnetic induction part. We adopted a second-order accurate linear ansatz reconstruction with a minmod limiter as well as the Harten–Lax–van Leer (HLL) approximate Riemann solvers (Harten, Lax, and van Leer, 1983) for the fluid part and the magnetic induction part, allowing more accurate calculations of wave speeds and therefore better resolution of waves (Ziegler, 2011). In time advance, the explicit second-order Runge–Kutta stepping with total variation diminishing was applied. For details, we refer to Feng, Zhang, and Zhou (2014).

3. Numerical Results

The global features of the modeled solar wind are displayed in Figure 1, a map in terms of the distributions of a) radial speed V_r , b) number density N , c) azimuthal speed V_ϕ , and

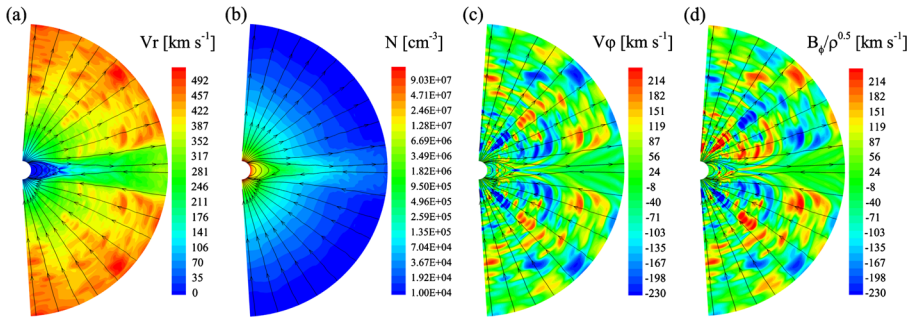


Figure 1 Distributions of radial speed V_r in km s^{-1} , number density N in cm^{-3} , azimuthal speed V_ϕ in km s^{-1} , and azimuthal magnetic field B_ϕ normalized in km s^{-1} in a meridional plane from 1 to 16 R_s at ≈ 40 h after the beginning of wave injection. The black lines denote the magnetic field lines.

d) azimuthal magnetic field B_ϕ in a meridional plane from 1 to 16 R_s after ≈ 40 h of wave injection. At that time, the wind has nearly reached a dynamic equilibrium. Panels c) and d) show the large-amplitude Alfvén waves. They significantly accelerate the plasma flow in the high-latitude region to form the fast wind (the yellow–orange–red zone in panel a)) with lower density (the bluish region off the green-equator in panel b)). From the mid- and high-latitudes, the fast wind stretches the magnetic field lines to form the open fields. At $\approx 5 R_s$, the stretched open fields become radial and occupy nearly all heliospheric latitudes. Meantime, at lower latitudes close to the equator, the plasma is slightly accelerated by the waves, and the slow wind with a higher density appears. The slow wind stretches the closed magnetic fields to form a helmet streamer with a sharp cusp structure at $\approx 4 R_s$. At the top of the streamer, a thin current sheet between different magnetic polarities is generated.

Further investigations of Alfvén waves reveal that they are most evident in the mid- and high-latitudes, but almost absent in the large region around the thin current sheet. Owing to the ponderomotive force, the persistent Alfvén waves in the mid- and high-latitudes accelerate the plasma there to form the high-speed flow. They also drive the compressive fluctuations, which nonlinearly steepen into shocks, as seen from the distributions of radial velocity and density. In the region around the equator, it should be noted that the transverse gradients (with respect to θ) of the Alfvén speed and those of the bulk velocity are large. Hence the phase mixing easily occurs there. When the Alfvén waves arrive there, they are very strongly damped by numerical resistivity, and only a small fraction of them can reach the thin current sheet (Grappin, Léorat, and Buttighoffer, 2000).

To investigate the acceleration of the two solar wind populations, Figure 2 presents the profiles of radial speed V_r in km s^{-1} , number density N in cm^{-3} , and azimuthal speed V_ϕ in km s^{-1} along heliocentric distance at latitudes $\theta = 5^\circ$ (red solid lines) and $\theta = 85^\circ$ (blue dashed lines) after ≈ 40 h of wave injection. The polar plasma at $\theta = 5^\circ$ is clearly accelerated throughout its way outward from near the Sun to reach $\approx 500 \text{ km s}^{-1}$ at the outlet. The acceleration starts from near the Sun, and the main acceleration interval terminates at $\approx 10 R_s$, similar to the previous volume heating model (Yang *et al.*, 2011). Accompanying the high-speed flow, the steepened shocks are clearly visible. For the equatorial wind, the quasi-stagnation region forms below $\approx 4 R_s$, which corresponds to a helmet streamer. Above the streamer, the plasma bulk speed starts to gradually increase to $\approx 250 \text{ km s}^{-1}$ by 16 R_s , with the main acceleration intervals terminating at $\approx 13 R_s$. At the outlet, the ratio between the highest (polar) and lowest (equatorial) wind velocity is ≈ 2 , agreeing with the observed

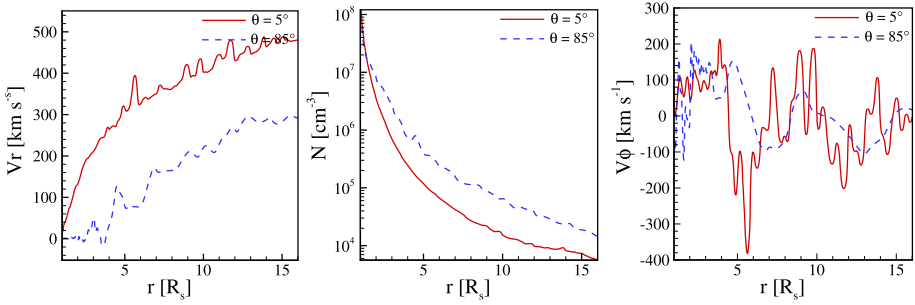


Figure 2 Profiles of radial speed V_r in km s⁻¹, number density N in cm⁻³, and azimuthal speed V_ϕ in km s⁻¹ along heliocentric distance at latitudes $\theta = 5^\circ$ (red solid lines) and $\theta = 85^\circ$ (blue dashed lines) at ≈ 40 h after the beginning of wave injection.

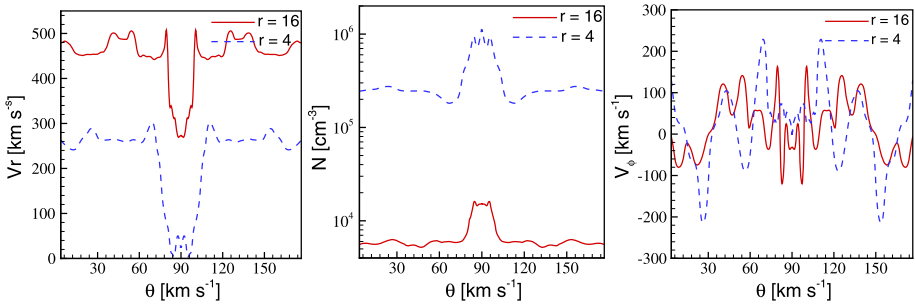


Figure 3 Profiles of radial speed V_r in km s⁻¹, number density N in cm⁻³, and azimuthal speed V_ϕ in km s⁻¹ along latitude at the heliocentric distances $r = 4 R_s$ (red solid lines) and $r = 16 R_s$ (blue dashed lines) at ≈ 40 h after the beginning of wave injection.

factor if extrapolated to 1 AU (Grappin, Léorat, and Habbal, 2002). For the high- and low-speed wind, the densities fall off steeply within $10 R_s$, and then they gently decrease.

To understand the role that the Alfvén wave plays in the acceleration, the pattern of the azimuthal velocity V_ϕ is plotted in Figure 2. It shows that for the fast polar outflow, the injected broadband Alfvén waves experience two changes. In the first change, the Alfvén wave amplitude increases from tens of km s⁻¹ near the Sun to hundreds of km s⁻¹ between the ranges from $\approx 4 R_s$ to $\approx 12 R_s$. Later, however, the Alfvén wave amplitude decreases. As noted by Grappin, Léorat, and Habbal (2002), this damping is associated with nonlinear steepening or a momentum transfer from waves to the bulk plasma flow. For the equatorial Alfvén waves of $\theta = 85^\circ$, high-frequency oscillations occur below $\approx 4 R_s$, which is at the closed field lines in the streamer as shown in Figure 1. We observe that these high-frequency waves decay before reaching the thin current sheet, leaving only the low-frequency and low-amplitude waves there.

To understand the transition between the modes, Figure 3 displays the profiles of radial speed V_r in km s⁻¹, number density N in cm⁻³, and azimuthal speed V_ϕ in km s⁻¹ along latitude at the heliocentric distances $r = 4 R_s$ (red solid lines) and $r = 16 R_s$ (blue dashed lines) after ≈ 40 h of wave injection. The figure again demonstrates the bimodal structure of both the wind and the Alfvén waves. From the polar open field to the equatorial current sheet, the wind transits from a fast polar stream to a slow equatorial stream. At the same time, the plasma number density increases almost four times at $4 R_s$ and three

Figure 4 Distribution of temperature T in K in a meridional plane from 1 to 16 R_s at ≈ 40 h after the beginning of wave injection. The black lines denote the magnetic fields lines.

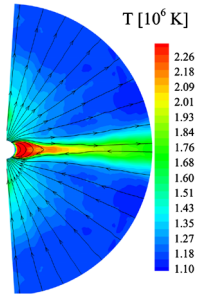
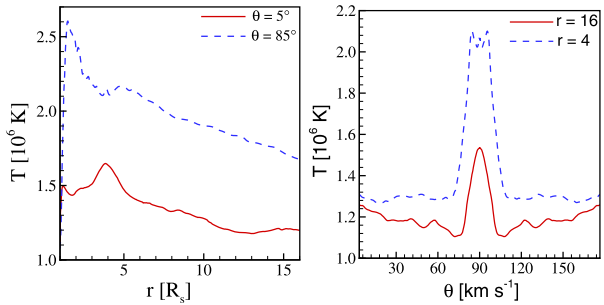


Figure 5 Profiles of temperature T in K along heliocentric distance (left) at latitudes $\theta = 5^\circ$ and $\theta = 85^\circ$ and along latitudes (right) at heliocentric distances $r = 8 R_s$ and $r = 16 R_s$ at ≈ 40 h after the beginning of wave injection. The vertical axes do not start at zero.



times at 16 R_s , while Alfvén waves transform from the large-amplitude waves into the very small-amplitude waves or almost disappear. At $r = 4 R_s$, the latitudinal extent of the near stagnation region for both the plasma and waves extends to $\theta = 82^\circ$, and the transition from the near-stagnation region to the region with the high-speed flow and the large-amplitude waves occurs gently. Nevertheless, at $r = 16 R_s$, both the bulk flow speed and the amplitude of waves increase rapidly with co-latitude. At $\theta = \pm 13^\circ$ is a sharp border separating the slow equatorial wind and the fast polar wind; it also separates the “blank” zone of waves and the zone with large-amplitude waves.

In addition to the outflow velocities, density, and Alfvén wave oscillation profiles illustrated above, we also investigated the temperature distribution shown in Figure 4. We see that both the fast and the slow wind become hotter than expected from the polytropic expansion. Evidently, plasma heating in the high-speed flow is due in large parts to MHD shocks (Orta, Huerta, and Boynton, 2003; Suzuki and Inutsuka, 2005), which stem from nonlinear Alfvén waves and are apparent in Figures 1 and 2. Conversely, the heating in the helmet streamer is due to the phase mixing (Ofman and Davila, 1995) and the plasma confinement in the closed field, which dramatically increase the temperature there to be maximal. The temperature within the thin current sheet is higher than in its surroundings.

Figure 5 presents the profiles of temperature T along heliocentric distance (left) at latitudes $\theta = 5^\circ$ and $\theta = 85^\circ$ and along latitudes (right) at the different heliocentric distances $r = 8 R_s$ and $r = 16 R_s$ after ≈ 40 h of wave injection. It shows that both winds undergo a rapid temperature increase away from the coronal base, and then behave differently. The temperature of the slow wind peaks at $\approx 2.6 \times 10^6$ K at $\approx 1.8 R_s$ and slowly decreases outward, while for the fast wind, the temperature ceases to rise earlier and is maintained at almost constant level until $\approx 3 R_s$. At this point, it starts to increase again, although slowly, until the peak at $\approx 4 R_s$; after the peak, the temperature begins to fall. At larger distance from the Sun, the temperature of the fast wind is lower than that of the slow-speed wind, indicating a possible lack of heating therein.

4. Summary and Discussion

We here investigated the global solar wind that is driven by explicit nonlinear Alfvén waves with a polytropic MHD model. A broadband spectrum of low-frequency Alfvén waves was launched from the base of the corona, with latitude-independent wave amplitudes. To resolve the waves clearly, high-resolution simulations were performed, and the numerical scheme was also carefully selected.

The model reproduced a fast and a slow solar wind. The ratio of their speeds agreed with *in situ* measurements. The bimodal winds were attributed to Alfvén waves; the waves accelerate the fast wind, the fast wind stretches the magnetic field lines, and in return, with such magnetic field configurations the waves can propagate without being strongly damped. On the other hand, near the equatorial plane, a strong gradient of the Alfvén speed and bulk velocity exists, and the phase mixing damps Alfvén waves there. As a result, the plasma is slightly accelerated and the slow solar wind forms. The acceleration of the fast wind starts from near the Sun, with the main acceleration interval terminating at $\approx 10 R_{\odot}$. The final speed of the fast wind at the outlet is $\approx 500 \text{ km s}^{-1}$, which is nearly twice as high as the speed of the slow wind. Accompanying the high-speed stream, the steepened shocks appear.

The numerical results also showed that the fast and slow wind are more intensely heated than is expected from the polytropic expansion. The heating of the fast wind is caused by steepened shocks, while heating in the slow wind is attributed to phase mixing. The profiles of temperature along heliocentric distance with different polar angles show that both winds undergo a rapid temperature increase away from the coronal base, and then behave differently. Far from the Sun, the temperature of the fast wind is lower than its surroundings, indicating a possible lack of heating in the fast wind.

We showed that the nonlinear Alfvén waves with latitude-independent amplitude well reproduce the velocity difference between the fast and slow solar wind. However, the resulting shock-heating in the fast wind seems not enough, which may be due to the simulation settings. Namely, the density at the coronal base was assumed to be constant in the present study. In realistic situations, the base density should be determined by the energy balance among heating, radiative cooling, and thermal conduction (Rosner, Tucker, and Vaiana, 1978; Withbroe, 1988), and more intense heating will lead to higher density at the coronal base. Therefore, the density at the coronal base in low-latitude regions will be higher because of the more intense heating by the Alfvén waves and also by chromospheric evaporation. On the other hand, the base density in high-latitude regions would be lower, where thermal conduction, related to the polytropic index there, becomes relatively more important as the conductive flux per mass increases. As a result, in a realistic situation the temperature in the fast wind will be higher than the temperature in the slow wind at a distant location, even though the temperature in the fast wind is lower near the Sun (Suzuki and Inutsuka, 2006). Another issue is related to the assumption of the constant polytropic index. The polytropic index, γ , in the present paper is a phenomenological replacement of thermal conduction. In realistic situations, the equivalent γ will vary in different locations. Especially in low-density regions, the polytropic index tends to be smaller, and the radial decrease of temperature is less steep (Steinolfson, Suess, and Wu, 1982), which may cause the higher temperature in the fast wind.

Other heating mechanisms may also need to be taken into account. Since the solar wind is highly turbulent, it is important to take the plasma heating through cascading of Alfvénic turbulence into account (Matthaeus *et al.*, 1999; Verdini and Velli, 2007). Recently, this topic has been investigated in detail (van der Holst *et al.*, 2014; Lionello *et al.*, 2014a,b; Cranmer, 2014; Usmanov, Goldstein, and Matthaeus, 2014). In the future, we plan to extend

the present work to a 3D case to self-consistently simulate the cascading of Alfvénic turbulence in the compressive MHD. The acceleration and heating evoked by Alfvén waves will be evaluated in detail.

In addition, this work may be improved by using the HLLD method because the HLL method is relatively numerically dissipative (Miyoshi and Kusano, 2005) and by including the chromosphere, where the nascent solar wind outflow is deemed to originate (He, Tu, and Marsch, 2007; He *et al.*, 2010a,b; Yang *et al.*, 2013). Finally, the solar wind plasma at 1 AU often shows complicated structures, *e.g.* various types of discontinuities. These complicated structures may play a role in the dissipation of Alfvén waves (Suzuki, 2008). It would be inspiring to numerically investigate their actual effects.

Acknowledgements This work is supported by NSFC under contract 41304133, 41474147, 41231069, 41222032, 41174148, 41421003, and 41204105. The numerical calculation has been completed on the computing system at Peking University.

References

- Alazraki, G., Couturier, P.: 1971, Solar wind acceleration caused by the gradient of Alfvén wave pressure. *Astron. Astrophys.* **13**, 380. [ADS](#).
- Barnes, A.: 1992, Theory of magnetohydrodynamic waves – The WKB approximation revisited. *J. Geophys. Res.* **97**, 12105. [DOI](#). [ADS](#).
- Belcher, J.W.: 1971, Alfvénic wave pressures and the solar wind. *Astrophys. J.* **168**, 509. [DOI](#). [ADS](#).
- Belcher, J.W., Davis, L. Jr.: 1971, Large-amplitude Alfvén waves in the interplanetary medium, 2. *J. Geophys. Res.* **76**, 3534. [DOI](#). [ADS](#).
- Chen, Y., Hu, Y.Q.: 2001, A two-dimensional Alfvén-wave-driven solar wind model. *Solar Phys.* **199**, 371. [DOI](#). [ADS](#).
- Cranmer, S.R.: 2012, Self-consistent models of the solar wind. *Space Sci. Rev.* **172**, 145. [DOI](#). [ADS](#).
- Cranmer, S.R.: 2014, Ensemble simulations of proton heating in the solar wind via turbulence and ion cyclotron resonance. *Astrophys. J. Suppl.* **213**, 16. [DOI](#). [ADS](#).
- Cranmer, S.R., van Ballegoijen, A.A., Edgar, R.J.: 2007, Self-consistent coronal heating and solar wind acceleration from anisotropic magnetohydrodynamic turbulence. *Astrophys. J. Suppl.* **171**, 520. [DOI](#). [ADS](#).
- Davila, J.M.: 1985, A leaky magnetohydrodynamic waveguide model for the acceleration of high-speed solar wind streams in coronal holes. *Astrophys. J.* **291**, 328. [DOI](#). [ADS](#).
- Esser, R., Habbal, S.R., Withbroe, G.L., Leer, E.: 1986, A two-fluid solar wind model with Alfvén waves – Parameter study and application to observations. *J. Geophys. Res.* **91**, 2950. [DOI](#). [ADS](#).
- Evans, R.M., Opher, M., Oran, R., van der Holst, B., Sokolov, I.V., Frazin, R., Gombosi, T.I., Vásquez, A.: 2012, Coronal heating by surface Alfvén wave damping: Implementation in a global magnetohydrodynamics model of the solar wind. *Astrophys. J.* **756**, 155. [DOI](#). [ADS](#).
- Feng, X., Zhang, M., Zhou, Y.: 2014, A new three-dimensional solar wind model in spherical coordinates with a six-component grid. *Astrophys. J. Suppl.* **214**, 6. [DOI](#). [ADS](#).
- Grappin, R., Léorat, J., Buttighoffer, A.: 2000, Alfvén wave propagation in the high solar corona. *Astron. Astrophys.* **362**, 342. [ADS](#).
- Grappin, R., Léorat, J., Habbal, S.R.: 2002, Large-amplitude Alfvén waves in open and closed coronal structures: A numerical study. *J. Geophys. Res.* **107**, 1380. [DOI](#). [ADS](#).
- Harten, A., Lax, P.D., van Leer, B.: 1983, A multi-state HLL approximate Riemann solver for ideal magnetohydrodynamics. *SIAM Rev.* **25**, 35. [DOI](#).
- He, J.-S., Tu, C.-Y., Marsch, E.: 2007, Can the solar wind originate from a quiet Sun region? *Astron. Astrophys.* **468**, 307. [DOI](#). [ADS](#).
- He, J.-S., Tu, C.-Y., Marsch, E.: 2008, Modeling of solar wind in the coronal funnel with mass and energy supplied at 5 Mm. *Solar Phys.* **250**, 147. [DOI](#). [ADS](#).
- He, J.-S., Marsch, E., Tu, C.-Y., Guo, L.-J., Tian, H.: 2010a, Intermittent outflows at the edge of an active region – A possible source of the solar wind? *Astron. Astrophys.* **516**, A14. [DOI](#). [ADS](#).
- He, J.-S., Tu, C.-Y., Tian, H., Marsch, E.: 2010b, Solar wind origins in coronal holes and in the quiet Sun. *Adv. Space Res.* **45**, 303. [DOI](#). [ADS](#).
- Hollweg, J.V.: 1973, Alfvén waves in a two-fluid model of the solar wind. *Astrophys. J.* **181**, 547. [DOI](#). [ADS](#).

- Hollweg, J.V.: 1978, Some physical processes in the solar wind. *Rev. Geophys. Space Phys.* **16**, 689. DOI. ADS.
- Hollweg, J.V.: 1990, On WKB expansions for Alfvén waves in the solar wind. *J. Geophys. Res.* **95**, 14873. DOI. ADS.
- Hollweg, J.V.: 2006, Drivers of the solar wind: then and now. *Phil. Trans. Roy. Soc. London* **364**, 505. DOI. ADS.
- Isenberg, P.A., Hollweg, J.V.: 1982, Finite amplitude Alfvén waves in a multi-ion plasma – Propagation, acceleration, and heating. *J. Geophys. Res.* **87**, 5023. DOI. ADS.
- Jacques, S.A.: 1977, Momentum and energy transport by waves in the solar atmosphere and solar wind. *Astrophys. J.* **215**, 942. DOI. ADS.
- Lau, Y.-T., Siregar, E.: 1996, Nonlinear Alfvén wave propagation in the solar wind. *Astrophys. J.* **465**, 451. DOI. ADS.
- Li, B., Li, X., Hu, Y.-Q., Habbal, S.R.: 2004, A two-dimensional Alfvén wave-driven solar wind model with proton temperature anisotropy. *J. Geophys. Res.* **109**, 7103. DOI. ADS.
- Lionello, R., Velli, M., Downs, C., Linker, J.A., Mikić, Z.: 2014a, Application of a solar wind model driven by turbulence dissipation to a 2D magnetic field configuration. *Astrophys. J.* **796**, 111. DOI. ADS.
- Lionello, R., Velli, M., Downs, C., Linker, J.A., Mikić, Z., Verdini, A.: 2014b, Validating a time-dependent turbulence-driven model of the solar wind. *Astrophys. J.* **784**, 120. DOI. ADS.
- Matsumoto, T., Suzuki, T.K.: 2014, Connecting the Sun and the solar wind: The self-consistent transition of heating mechanisms. *Mon. Not. Roy. Astron. Soc.* **440**, 971. DOI. ADS.
- Matthaeus, W.H., Zank, G.P., Oughton, S., Mullan, D.J., Dmitruk, P.: 1999, Coronal heating by magneto-hydrodynamic turbulence driven by reflected low-frequency waves. *Astrophys. J. Lett.* **523**, L93. DOI. ADS.
- McComas, D.J., Barraclough, B.L., Funsten, H.O., Gosling, J.T., Santiago-Muñoz, E., Skoug, R.M., Goldstein, B.E., Neugebauer, M., Riley, P., Balogh, A.: 2000, Solar wind observations over Ulysses' first full polar orbit. *J. Geophys. Res.* **105**, 10419. DOI. ADS.
- McComas, D.J., Elliott, H.A., Schwadron, N.A., Gosling, J.T., Skoug, R.M., Goldstein, B.E.: 2003, The three-dimensional solar wind around solar maximum. *Geophys. Res. Lett.* **30**, 1517. DOI. ADS.
- Miyoshi, T., Kusano, K.: 2005, A multi-state HLL approximate Riemann solver for ideal magnetohydrodynamics. *J. Comput. Phys.* **208**, 315. DOI. ADS.
- Ofman, L.: 2004, Three-fluid model of the heating and acceleration of the fast solar wind. *J. Geophys. Res.* **109**, 7102. DOI. ADS.
- Ofman, L.: 2010, Wave modeling of the solar wind. *Living Rev. Solar Phys.* **7**(4). DOI. ADS.
- Ofman, L., Davila, J.M.: 1995, Alfvén wave heating of coronal holes and the relation to the high-speed solar wind. *J. Geophys. Res.* **100**, 23413. DOI. ADS.
- Ofman, L., Davila, J.M.: 1997, Solar wind acceleration by solitary waves in coronal holes. *Astrophys. J.* **476**, 357. ADS.
- Ofman, L., Davila, J.M.: 1998, Solar wind acceleration by large-amplitude nonlinear waves: Parametric study. *J. Geophys. Res.* **103**, 23677. DOI. ADS.
- Oran, R., van der Holst, B., Landi, E., Jin, M., Sokolov, I.V., Gombosi, T.I.: 2013, A global wave-driven magnetohydrodynamic solar model with a unified treatment of open and closed magnetic field topologies. *Astrophys. J.* **778**, 176. DOI. ADS.
- Orta, J.A., Huerta, M.A., Boynton, G.C.: 2003, Magnetohydrodynamic shock heating of the solar corona. *Astrophys. J.* **596**, 646. DOI. ADS.
- Rosner, R., Tucker, W.H., Vaiana, G.S.: 1978, Dynamics of the quiescent solar corona. *Astrophys. J.* **220**, 643. DOI. ADS.
- Steinolfson, R.S., Suess, S.T., Wu, S.T.: 1982, The steady global corona. *Astrophys. J.* **255**, 730. DOI. ADS.
- Suzuki, T.K.: 2008, Coronal heating and wind acceleration by nonlinear Alfvén waves – Global simulations with gravity, radiation, and conduction. *Nonlinear Process. Geophys.* **15**, 295. ADS.
- Suzuki, T.K., Inutsuka, S.-I.: 2005, Making the corona and the fast solar wind: A self-consistent simulation for the low-frequency Alfvén waves from the photosphere to 0.3 AU. *Astrophys. J. Lett.* **632**, L49. DOI. ADS.
- Suzuki, T.K., Inutsuka, S.-I.: 2006, Solar winds driven by nonlinear low-frequency Alfvén waves from the photosphere: Parametric study for fast/slow winds and disappearance of solar winds. *J. Geophys. Res.* **111**, A06101. DOI. ADS.
- Tu, C.-Y., Marsch, E.: 1995, MHD structures, waves and turbulence in the solar wind: Observations and theories. *Space Sci. Rev.* **73**, 1. DOI. ADS.
- Usmanov, A.V., Goldstein, M.L., Matthaeus, W.H.: 2014, Three-fluid, three-dimensional magnetohydrodynamic solar wind model with eddy viscosity and turbulent resistivity. *Astrophys. J.* **788**, 43. DOI. ADS.
- Usmanov, A.V., Goldstein, M.L., Besser, B.P., Fritzer, J.M.: 2000, A global MHD solar wind model with WKB Alfvén waves: Comparison with Ulysses data. *J. Geophys. Res.* **105**, 12675. DOI. ADS.

- van der Holst, B., Sokolov, I.V., Meng, X., Jin, M., Manchester, W.B. IV, Tóth, G., Gombosi, T.I.: 2014, Alfvén wave solar model (AWSOM): Coronal heating. *Astrophys. J.* **782**, 81. <http://stacks.iop.org/0004-637X/782/i=2/a=81>.
- Verdini, A., Velli, M.: 2007, Alfvén waves and turbulence in the solar atmosphere and solar wind. *Astrophys. J.* **662**, 669. DOI. ADS.
- Wang, X., He, J., Tu, C., Marsch, E., Zhang, L., Chao, J.-K.: 2012, Large-amplitude Alfvén wave in interplanetary space: the wind spacecraft observations. *Astrophys. J.* **746**, 147. DOI. ADS.
- Withbroe, G.L.: 1988, The temperature structure, mass, and energy flow in the corona and inner solar wind. *Astrophys. J.* **325**, 442. DOI. ADS.
- Woo, R., Martin, J.M.: 1997, Source regions of the slow solar wind. *Geophys. Res. Lett.* **24**, 2535. DOI. ADS.
- Yang, L.-P., Feng, X.-S., Xiang, C.-Q., Jiang, C.-W.: 2011, Numerical validation and comparison of three solar wind heating methods by the SIP-CESE MHD model. *Chin. Phys. Lett.* **28**, 039601. DOI. ADS.
- Yang, L., He, J., Peter, H., Tu, C., Chen, W., Zhang, L., Marsch, E., Wang, L., Feng, X., Yan, L.: 2013, Injection of plasma into the nascent solar wind via reconnection driven by supergranular advection. *Astrophys. J.* **770**, 6. <http://stacks.iop.org/0004-637X/770/i=1/a=6>.
- Ziegler, U.: 2011, A semi-discrete central scheme for magnetohydrodynamics on orthogonal-curvilinear grids. *J. Comput. Phys.* **230**, 1035. DOI. ADS.